Atmospheric simulation-based precipitation datasets outperform satellite-based products in closing basin-wide water budget in the eastern Tibetan Plateau

Article *in* International Journal of Climatology · April 2022

DOI: 10.1002/joc.7642

CITATIONS
16

READS
366

7 authors, including:

Yaozhi Jiang
University of Electronic Science and Technology of China
28 PUBLICATIONS **459** CITATIONS
SEE PROFILE

Kun Yang
Tsinghua University
351 PUBLICATIONS **23,736** CITATIONS
SEE PROFILE

Yingying Chen
Institute of Tibetan Plateau Research CAS
92 PUBLICATIONS **6,621** CITATIONS
SEE PROFILE

Jiang Yaozhi (Orcid ID: 0000-0002-6051-755X)
Yang Kun (Orcid ID: 0000-0002-0809-2371)

Atmospheric simulation-based precipitation datasets outperform satellite-based products in closing basin-wide water budget in the eastern Tibetan Plateau

Yaozhi Jiang[1,2,3], Kun Yang[3,1*], Xiaodong Li[4], Wenjiang Zhang[4], Yan Shen[5], Yingying Chen[1], Xin Li[1]

[1] National Tibetan Plateau Data Center, State Key Laboratory of Tibetan Plateau Earth System and Resource Environment, Institute of Tibetan Plateau Research, Chinese Academy of Sciences, Beijing 100101, China.

[2] University of Chinese Academy of Sciences, Beijing 100049, China

[3] Department of Earth System Science, Ministry of Education Key Laboratory for Earth System Modeling, Institute for Global Change Studies, Tsinghua University, Beijing 100084, China.

[4] State Key Laboratory of Hydraulics and Mountain River Engineering, Sichuan University, Chengdu 610065, China

[5] National Meteorological Information Center, China Meteorological Administration, Beijing 100081, China

Corresponding author: Kun Yang (yangk@tsinghua.edu.cn)

Acknowledgments: This work was supported by National Key Research and Development Program of China (Grant No. 2018YFA0605400), NSFC Basic Science Center for Tibetan Plateau Earth System (Grant No. 41988101) and the International Partnership Program of Chinese Academy of Sciences (Grant No. 183311KYSB20200015)

This article has been accepted for publication and undergone full peer review but has not been through the copyediting, typesetting, pagination and proofreading process which may lead to differences between this version and the Version of Record. Please cite this article as doi: 10.1002/joc.7642

Abstract

Satellite-based precipitation products (SBPs) have been widely used in hydrological applications in recent decades but may contain large uncertainties in mountainous regions. Atmospheric simulation-based datasets (ABDs) have been greatly improved in recent years, but their applications in mountainous hydrology are rare and need further validation. This study compares the performance of three SBPs and two ABDs in the mountainous Minjiang River basin, focusing on their potential for closing the basin-wide water budget. The three SBPs include the China Merged Precipitation Analysis (CMPA), the Integrated Multi-satellitE Retrievals for Global Precipitation Measurement (IMERG) and the Global Satellite Mapping of Precipitation (GSMaP); the two ABDs are the 5th generation Reanalysis product of the European Centre for Medium Range Weather Forecasts (ERA5) and the High Asia Refined Analysis Version 2 (HAR V2). The five products are validated with rain gauge data and results show that all the five products except IMERG can generally reproduce the spatial pattern and elevation dependence of observed precipitation. Particularly, precipitation amount in the two ABDs is close to gauge observations in the low elevations, but much more than the gauge observations in areas with a sharp rise in elevations. Assessment of water budget shows that all SBPs yield severe negative water imbalance (greater than 50.0% of corresponding runoff) at most sub-basins, while the ABDs can better close the water budget with water imbalance values between ±30.0% in most sub-basins, respectively. Further analyses show that large relative differences between SBPs and ABDs mainly occur in areas with large topographical relief and in winter, which is likely because the ABDs outperform the SBPs in capturing orographic precipitation in complex terrain and solid precipitation in winter.

Keywords: precipitation; atmospheric simulation; evaluation; water budget; complex terrain

1. Introduction

The Tibetan Plateau (TP) is the main source of many Asia rivers, and runoff from the TP contributes significantly to downstream water resources that are vital to agriculture, industry and human life. Meanwhile, this region is subjected to strong water and energy exchange between the land surface and atmosphere due to the distinctive natural environment. Quantifying the basin-wide water budget in the TP is of great importance for water resources management, prevention of water-related disasters and understanding of land-surface hydrological processes. Among the many water budget components, precipitation is a key element but with large uncertainties in the TP because monitoring networks are sparse and unevenly distributed here. Gridded precipitation products fill the gap caused by sparse ground observations, making it possible to understand the water budget in ungauged regions like the TP. The gridded precipitation products mainly include gauge-based products, satellite-based products and reanalysis or atmospheric simulation-based products.

The gauge-based and satellite-based precipitation products (SBPs) are most widely used in recent decades because they are derived from observations and considered to be more reliable. These products include GPCC (the Global Precipitation Climatology Centre data; Becker *et al*., 2013), APHRODITE (Asian Precipitation-Highly-Resolved Observational Data Integration Towards Evaluation; Yatagai *et al.,* 2012), TMPA (TRMM Multisatellite Precipitation Analysis; Huffman *et al*., 2007), GSMaP (Global Satellite Mapping of Precipitation; Kubota *et al*., 2006), IMERG (Integrated Multi-satellitE Retrievals for Global Precipitation Measurement; Huffman *et al*., 2019), etc. They play an important role in understanding hydrological processes, flood forecasting and water resources management (Beighley *et al*., 2009; Belabid *et al.,* 2019; Chiang *et al*., 2007; Hong *et al*., 2007; Hughes, 2006; Siddique-E-Akbor *et al*., 2014;; Wang *et al*., 2005; Wu *et al*., 2014; Yang *et al*., 2017; Yilmaz *et al*., 2005). In the TP, the gauge-based and satellite-based products have also been widely applied (Li *et al*., 2015; Liu *et al*., 2017; Lu and Yong, 2018; Su *et al*., 2008), but many studies pointed out that these products perform poor in capturing solid precipitation (Li *et al.*, 2020; Lu and Yong, 2018) and reflecting precipitation variability in complex-terrain regions (Immerzeel *et al*., 2015; Shen *et al.*, 2014a).

The applications of reanalysis data or atmospheric simulation-based precipitation (ABDs) for

hydrological research have been rare in the past decades, mainly due to their coarse spatial resolution and large uncertainties. The ERA5 reanalysis (Hersbach *et al*., 2020) was recently released by the European Centre for Medium Range Weather Forecasts (ECMWF), which incorporated many improvements compared with the previous reanalysis data (Chen *et al*., 2020; Hersbach *et al*., 2020; Keller and Wahl, 2020; Tarek *et al.*, 2020) and can reasonably represent the spatialtemporal variability of precipitation (Hu and Yuan, 2021; Yuan *et al.*, 2021). Moreover, it has a fine horizontal resolution of 0.25°. These improvements make it competitive with gauge and satellite-based precipitation products in hydrological applications. In addition, dynamical downscaling precipitation datasets based on Regional Climate Models (RCMs) are arising recent years, such as High Asia Refined Analysis (HAR; Maussion *et al*., 2014) and High Asia Refined Analysis version 2 (HAR V2; Wang *et al*., 2020). Previous studies showed that the atmospheric simulation-based datasets have good performance in capturing precipitation seasonality and spatial variability in complex terrain (Maussion *et al*., 2014; Wang *et al*., 2018). Therefore, they are expected to have potential capabilities in hydrological applications in the TP, but these capabilities need to be validated.

In the TP, some studies have already tested the performance of atmospheric simulation-based precipitation in hydrological applications, e.g. Pritchard *et al.* (2019) evaluated the accuracy of precipitation from HAR with basin runoff in the upper Indus and the results showed that precipitation from HAR is consistent with the sum of runoff and evapotranspiration at most basins; Li *et al*. (2020) compared multiple precipitation products in upper Indus and showed that HAR can better reflect the annual precipitation amount and thus better close the water budget than other gauge or satellite-based products; Gao *et al*. (2020) simulated the snow cover with multiple precipitation datasets in the southeastern TP and found that the simulated result forced by precipitation from high-resolution atmospheric simulation can reproduce the observed snow cover well. The existing assessments are mainly conducted in the western and southern TP where snow is dominated, focusing on the potential of the atmospheric model in capturing solid precipitation that is challenging for gauge and satellite-based precipitation products (Lundquist *et al*., 2019; Maussion *et al*., 2014; Wang *et al*., 2018). However, atmospheric models may behave differently in different regions due to the uncertainties in parameterizations (He *et al*., 2015; Sun *et al*., 2021). Therefore, there is still a need to assess

atmospheric simulation-based precipitation for hydrological applications in the eastern TP that is characterized by complex terrain and monsoon climate.

In this regard, the main objectives of this study are to investigate the ability of ABDs in closing basin-wide water budget in a monsoon-dominated mountainous basin and compare their performance with the widely used SBPs. We focus on the Minjiang River basin (Figure 1) located at the eastern margin of the TP. This basin has an area of 126333 km^2 and is characterized by complex terrain. The Chengdu plain located in the southeastern part of the river basin has an elevation lower than 500 m a.s.l., while the Minya Konka, the highest mountain in this area, has an elevation higher than 7000 m a.s.l. Elevations over 2000 m a.s.l. account for more than 70% of the total basin area. Due to the sharp increase in elevations, orographic precipitation is evident in this basin, causing that this area is one of China's most famous precipitation hotspots, and includes Ya'an which is called the "Sky Leak" or "Rainy City". The high precipitation provides critical water resources for the region and downstream areas. The average runoff of the Wutongqiao station (the outlet of the Minjiang River basin) is 2224.8 m^3/s (averaged over the period from 2008 to 2017). According to Cui et al. (2012), the Minjiang River basin provides about 8.9% water yield for the upper Yangtze River. Meanwhile, steep terrain has brought abundant waterpower resources for this region and thus many water conservancy projects have been built in the past decades. However, due to the steep terrain, rain gauges are mainly located in the lowland areas or valleys and obtaining spatially distributed precipitation data based on rain gauge is challenging, which prevents further understanding of the hydrological processes in this region. Therefore, gridded precipitation products are expected to play an important role in the management of water resources and understanding hydrological processes in the mountainous Minjiang River basin.

2. Description of datasets

2.1 Precipitation datasets

2.1.1 Rain gauge data

The rain gauge data was collected from the office of Flood Control and Drought Relief Headquarters of Sichuan Province, China. The rain gauge network was set up and maintained by the Hydrological Bureau of the Ministry of Water Resources in China. The rain gauge data were

automatically recorded at an interval of one hour with tipping bucket rain gauges with no wind shield. The rain gauge has a precision of 0.5 mm and can measure the maximum precipitation intensity of 4 mm/min. The total annual precipitation and repetition of constant values were checked manually. In addition, the quality control steps for daily precipitation proposed by Serrano-Notivoli *et al*. (2017) were applied to this dataset, in which the suspect values were flagged by comparing the measurements with those from their nearest 10 rain gauges. Detailed criteria for defining the suspect values can be found in Serrano-Notivoli *et al*. (2017). Eventually, data from 375 rain gauges in 2017 were used for the analysis. Each rain gauge has missing values less than 9.0% of the total records. When calculating the monthly and annual precipitation, the data gaps were filled using the method proposed by Liu *et al*. (2018), in which the Bayesian linear regression for the interpolation of station data was used and proved to be superior to the inverse distance weighted method, local polynomial method and Kriging method. Figure 1b shows that the rain gauges are unevenly distributed, with more in low-altitude areas and less in high-altitude areas.

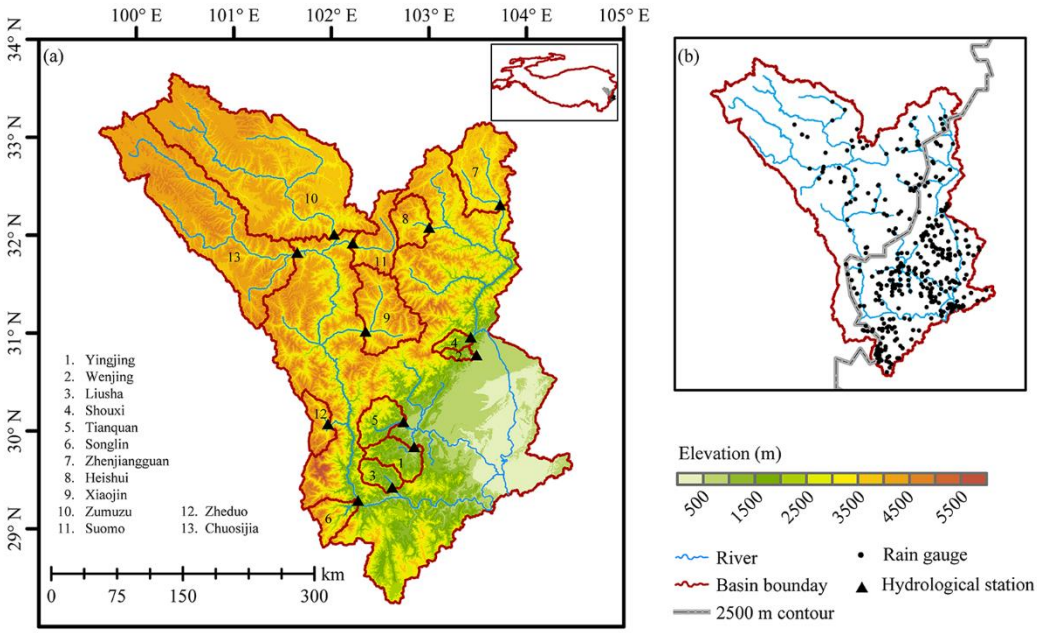

Figure 1 (a) Location and topography of the study area and 13 sub-basins of the Minjiang River basin, for which the water budget is analyzed. (b) Distribution of rain gauges.

2.1.2 Gridded precipitation products

Five gridded precipitation products were selected in this study. These products are ERA5, HAR V2, CMPA (Shen *et al.*, 2014b), IMERG and GSMaP.

ERA5 is the latest global reanalysis dataset produced by ECMWF, which provides dozens of atmospheric and land surface variables. The ERA5 is produced using the advanced 4D-Var assimilation system, by which extensive data from ground observation, atmospheric sounding and satellite observation are assimilated. Compared with previous reanalysis data, the ERA5 has many improvements in terms of both spatiotemporal resolution and accuracy (Chen *et al*., 2020; Hersbach *et al*., 2020; Keller and Wahl, 2020). The precipitation from ERA5 with a spatial resolution of 0.25°×0.25° was used in this study, which can be accessed from https://cds.climate.copernicus.eu/cdsapp#!/dataset/reanalysis-era5-single-levels?tab=overview.

HAR V2 was produced by dynamically downscaling ERA5 reanalysis using the WRF model. It covers the High Mountain Asia with the highest spatial resolution of 10 km. Unlike ERA5, no ground or satellite observations are assimilated in the HAR V2, thus, the performance of HAR V2 highly depends on the boundary conditions (i.e. the inputs provided by ERA5) and the WRF model. Details about the model configuration and the parameterization can be found in Wang *et al*. (2020), and the data can be downloaded from ftp://ftp.klima.tu-berlin.de/HAR/V2.

CMPA is a merged product that has combined the rainfall data from more than 30000 automatic weather stations in China and the CMORPH (CPC MORPHing technique; Joyce *et al*., 2004) precipitation product. Three steps are involved to produce the CMPA product: first, the rain gauge data are interpolated to regular grids using improved optimal interpolation (OI) (Xie *et al*., 2007) and the CMORPH estimates are resampled to the same spatiotemporal resolution; second, the resampled CMORPH data are corrected by matching its probability density function (PDF) with that of the interpolated gauge data; finally, the corrected CMORPH and interpolated gauge data are merged based on the OI method. More details about the algorithm and product are available in Shen *et al*. (2014b). This dataset can be obtained from National Meteorological Information Center of China.

GPM (Global Precipitation Measurement) utilizes a constellation of satellites to provide comprehensive detection of precipitation (Hou *et al*., 2014). Compared to the TRMM instruments, the application of dual-frequency precipitation radar (DPR) and GPM Microwave Imager (GMI) in the GPM Core Observatory satellite leads to more accurate detection of light and solid precipitation. Multiple microwave and infrared algorithms are combined to produce the IMERG products (Huffman

et al, 2019). The half-hourly Final Run product Version 6 is used in our study, and is available from the Earthdata Search (https://search.earthdata. nasa.gov/ search).

The GSMaP project is supported by the JAXA Precipitation Measuring Mission Science Team and has developed a new retrieval algorithm to estimate precipitation from available microwave and infrared sensors by adding information from the GPM core GMI. This new algorithm has been applied in the production of GSMaP V6. Moreover, the GSMaP V6 has included an orographic precipitation correct method (developed by Shige *et al*. (2013) and modified by Yamamoto and Shige (2015)) to improve the rainfall estimates in complex-terrain areas. A gauge-calibrated version of GSMaP V6, named GSMaP_Gauge V6, is used in our study. It is worth noting that GSMaP_gauge V6 is only designed for the GPM era, and a reanalysis product (GSMaP_Gauge_NRL) is provided for the period before March 2014. Because long-term precipitation data are needed for water budget analysis in our study, the GSMaP_Gauge_NRL V6 product is also used for the period before March 2014.

A summary of the spatiotemporal resolution and coverage of these products is given in Table 1.

Table 1 Basic information of the gridded precipitation products (P) and evapotranspiration products (ET) used in this study.

	Product	Spatial resolution	Temporal resolution	Spatial Coverage
P	ERA5	0.25°×0.25°	1 hour	Global
	HAR V2	10 km×10 km	1 hour	High Mountain Asia
	CMPA	0.1°×0.1°	1 hour	Chinese Mainland
	IMERG V06	0.1°×0.1°	0.5 hour	Global
	GSMaP_gauge V06	0.1°×0.1°	1 hour	60°S - 60°N
ET	ERA5	0.25°×0.25°	1 month	Global
	HAR V2	10 km×10 km	1 month	High Mountain Asia
	GLDAS_NOAH025	0.25°×0.25°	1 month	60°S - 90°S
	GLEAM v3.3a	0.25°×0.25°	1 month	Global
	MOD16A3 V06	500 m × 500 m	1 year	Global
	GLASS	0.05°×0.05°	8 day	Global

2.2 Evapotranspiration (ET) datasets

Evapotranspiration is an important component of the water budget. It has great spatial variability, but there are no direct observations of evapotranspiration in the Minjiang River basin. Instead, six ET products were used for basin-wide water budget analysis in this study, including estimates from ERA5 and HAR V2, and four independent products (GLDAS, GLEAM, MODIS and GLASS). The four independent products are briefly described below.

The GLDAS dataset is produced using the NASA Global Land Data Assimilation System which aims at providing optimal land fields of land surface states and fluxes (Rodell *et al*., 2004). Various land surface models have been applied in the NASA Global Land Data Assimilation System. The monthly data obtained by driving the Noah land surface model (GLDAS_NOAH025_M 2.1) were used in this study.

The Global Land Evaporation Amsterdam Model (GLEAM) calculates various components of evapotranspiration using a set of algorithms (Miralles *et al*., 2011). In our study, the GLEAM v3.3a dataset was employed for water budget analysis; this is produced using the radiation and air temperature data from ERA5 as its forcing data.

The evapotranspiration of MODIS (Moderate Resolution Imaging Spectroradiometer; Mu *et al*., 2013) is derived from the Penman-Monteith equation (Monteith, 1965), by taking the satellite data (vegetation property dynamics, albedo, land cover, etc.) from MODIS and meteorological data from MERRA (Rienecker *et al*., 2011) as input. The yearly MOD16A3 version 6 dataset was used in this study, which has a spatial resolution of 500 m.

The ET of GLASS (Global Land Surface Satellite Product; Yao *et al*., 2014) is produced based on satellite data of MODIS/AVHRR and reanalysis data of MERRA. Different from the ET of MODIS in which only one algorithm is adopted, GLASS uses a Bayesian method to merge the ETs calculated from six different algorithms. In this study, the GLASS ET with a spatial resolution of 0.05°×0.05° and temporal resolution of 8 day was used.

The four ET products have different spatial resolution but this is not of great concern because the basin-averaged ET will be used for the water budget calculation.

2.3 Runoff

Daily runoff data for 13 sub-basins (Figure 1a) of the Minjiang River basin were collected from the Hydrological Bureau of the Ministry of Water Resources in China. The temporal coverage of the runoff data in each sub-basin is shown in Table 2. All the sub-basins have days with missing data less than 5.0% of the total number of days in the analysis periods. The missing data were filled using simple linear interpolation.

Table 2 Basic information of the 13 sub-basins in the Minjiang River basin.

Sub-basin	Basin name	Basin area（km^2）	Mean Elevation（m）	Temporal coverage of runoff data	Percentage of missing records (%)
1	Yingjing	1694.5	1786.3	2008-2017	1.0
2	Wenjing	354.1	1864.5	2014, 2016, 2017	4.3
3	Liusha	1076.0	2069.6	2013-2017	3.9
4	Shouxi	562.7	2267.0	2015-2017	1.9
5	Tianquan	1720.7	2408.8	2008-2017	1.0
6	Songlin	1443.9	3499.5	2013-2017	2.7
7	Zhenjiangguan	4471.2	3625.7	2014-2017	1.6
8	Heishui	1716.2	3850.4	2013-2017	1.3
9	Xiaojin	4253.7	3954.5	2015, 2017	1.6
10	Zumuzu	19923.2	3964.5	2013-2016	1.9
11	Suomo	2529.9	3964.5	2015-2017	1.3
12	Zheduo	1352.4	4178.4	2014-2017	1.6
13	Chuosijia	14824.8	4186.0	2016-2017	1.5

2.4 Other datasets

To explore the relations between the performance of precipitation products and topography, elevation data from the Shuttle Radar Topographic Mission (SRTM; Farr *et al.*, 2007) was used in this study. The elevation data has a horizontal resolution of 90 m. In addition, the albedo data from the MODIS (MCD43C3 Version 6; Schaaf *et al.*, 2002) was also used in this study, which has a temporal resolution of 1 day and a horizontal resolution of 0.05°.

3. Methods

In this study, the water budget in the Minjiang River basin was investigated using the five gridded precipitation products. Under natural conditions, the water budget of a specific river basin can be described using the following formula:

$$\Delta S = P + R_{in} - R_{out} - ET \,, \tag{1}$$

Where ΔS is the water storage change, P is the basin-averaged precipitation, R_{in} and R_{out} are the inflow and outflow of the basin, respectively, and ET is the basin-averaged evapotranspiration.

In mountainous regions like the Minjiang River basin, due to the steep slopes and limited water storage capacity of soil in these regions, the water storage change (ΔS) can be assumed to be zero at the annual or multi-year scale (Wang *et al*., 2015; Ye *et al*., 2012; Zhang *et al*., 2018). For a closed headwater watershed, the incoming runoff (R_{in}) is also equal to zero. Thus, relative water imbalance (ΔW) at annual or multi-year scale due to errors in water budget components can be defined as follows:

$$\Delta W = \frac{P - ET - R_{out}}{R_{out}} \times 100\% \,, \tag{2}$$

In this study, the water budget analyses were limited to 13 sub-basins shown in Figure 1a and Table 2. These sub-basins are all headwater basins without incoming runoff and no reservoirs with multi-year regulation capacity and large water diversion projects exist in these basins. There are some gate dams in some sub-basins, such as the Tianquan River basin, which can redistribute the daily discharge, but have small impacts on the annual or multi-year average runoff.

The water budget was analyzed based on multi-year average precipitation, runoff and ET. The period for averaging the water budget components is corresponding to the temporal coverage of runoff data in each sub-basin (as shown in Table 2), for example, the water budget analysis for the Yingjing River basin was conducted based on the multi-year average values during the period from 2008 to 2017. This leads to inconsistent analysis periods for different sub-basins, however, it is appropriate because our focus is to compare the performance of different precipitation products rather than investigate the inter-annual variations of water budget components.

The basin-average precipitation and ET were then calculated based on the gridded multi-year average values. Given that some sub-basins have small basin areas and some precipitation and ET

products have a coarse horizontal resolution. The basin-average precipitation and ET were calculated using an area-weighted method, in which the gridded precipitation within a basin was averaged with weighted by grid/sub-grid area.

In this study, the amount of ET in each sub-basin was represented using the ensemble mean of the estimates from six ET products mentioned in section 2.2, and the ranges between maximum and minimum estimates of the six products were used to represent the uncertainties in ET.

4. Results

4.1 Spatial pattern of precipitation

The total amounts of precipitation in 2017 from the gauge data and precipitation products are compared in Figure 2. Figure 2a reveals great spatial variability of precipitation in gauge observations, with annual precipitation ranging from about 480 mm to more than 2300 mm. In general, a large amount and great spatial variability of precipitation are observed in the central part of the Minjiang River basin that is generally along the 2500 m elevation contour in the eastern TP. This is because this region is located at the windward slopes and has a sharp increase in altitude, which usually leads to enhanced precipitation in these regions. In the lowland Chengdu Plain and the northwestern part of the Minjiang River basin, where the topography is relatively flat, precipitation is relatively small and shows less heterogeneity in space. This indicates that local topography greatly influences the distribution of precipitation in mountainous regions.

As shown in Figure 2, among the five gridded precipitation products, ERA5, HAR V2 and CMPA can generally reproduce the spatial pattern of observed precipitation, clearly revealing the relatively small precipitation amount in the east and northwest but the large amount in the central and southwest parts of the Minjiang River basin. GSMaP can also generally identify the precipitation center. However, IMERG yields a large amount of precipitation in the Chengdu Plain. In the northwest and southwest parts of the Minjiang River basin, ERA5 and HAR V2 show more precipitation than the three SBPs. Particularly, it can be seen that the gauge observations vary greatly even within a grid cell of gridded precipitation products, indicating that coarse-resolution gridded precipitation products are unable to capture the fine-scale variability of precipitation and the evaluation of gridded precipitation products based on rain gauge data may suffer from scale mismatch and poor

representativeness of rain gauges (Li, 2014).

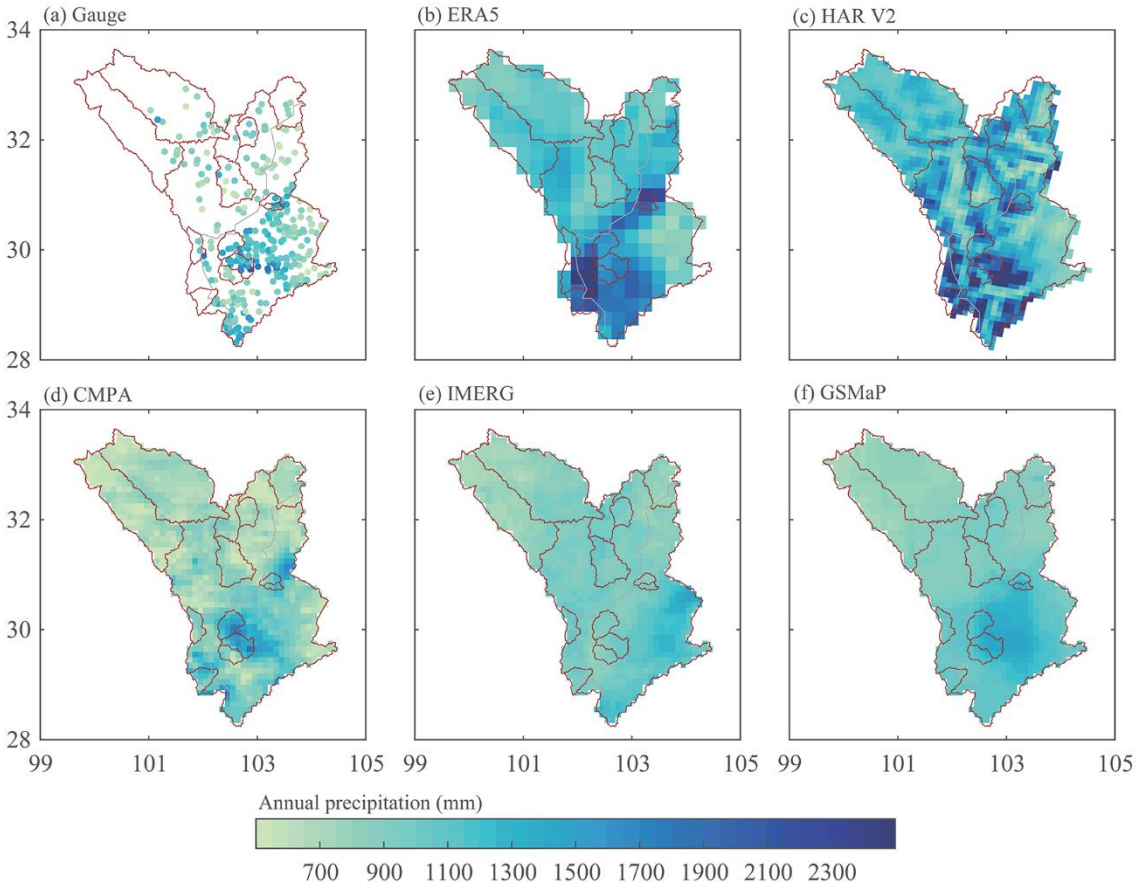

Figure 2 Spatial distribution of the annual precipitation in 2017 in the Minjiang River basin for gauge observation and five precipitation products.

4.2 Seasonal pattern of precipitation

Figure 3 compares the average monthly precipitation from the five gridded precipitation products during 2008-2017. The monthly precipitation was averaged across all grid cells in the Minjiang River basin using the area-weighted method. It can be seen that all products generally show similar patterns. Precipitation from the three SBPs (CMPA, IMERG and GSMaP) is close to each other, with maximum precipitation in July, which is lower than 180.0 mm. The two ABDs (ERA5 and HAR V2) have higher precipitation than the three SBPs in all months, particularly in summer. The amount of precipitation from ERA5 and HAR V2 in July is 240.5 mm and 285.7 mm, respectively.

The precipitation from the five gridded precipitation products is compared in different sub-basins of the Minjiang River basin with respect to four seasons and is displayed in Figure 4. In Figure 4, the mean elevation of each sub-basin on the horizontal axis increases from left to right. Generally, the

two ABDs unexceptionally have higher precipitation than the three SBPs in all sub-basins and all seasons. Particularly, it can be seen from Figure 4 that HAR V2 tends to have higher precipitation than ERA5 in high-elevation sub-basins and in summer, which may be caused by the difference in the parameterization and model configuration between them. For sub-basins located at relatively low elevations, the differences between these products are quite large in all seasons. The large differences are likely related to great spatial variability of topography in these sub-basins, which will be discussed in section 5.1. In relatively highland sub-basins, the differences among these gridded precipitation products are small but vary between different seasons with large relatively differences in winter.

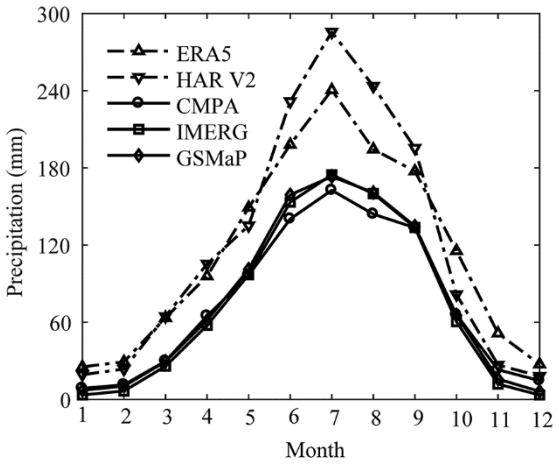

Figure 3 Comparison of the monthly precipitation from the five products averaged across the Minjiang River basin. The monthly precipitation is averaged over the period from 2008 to 2017.

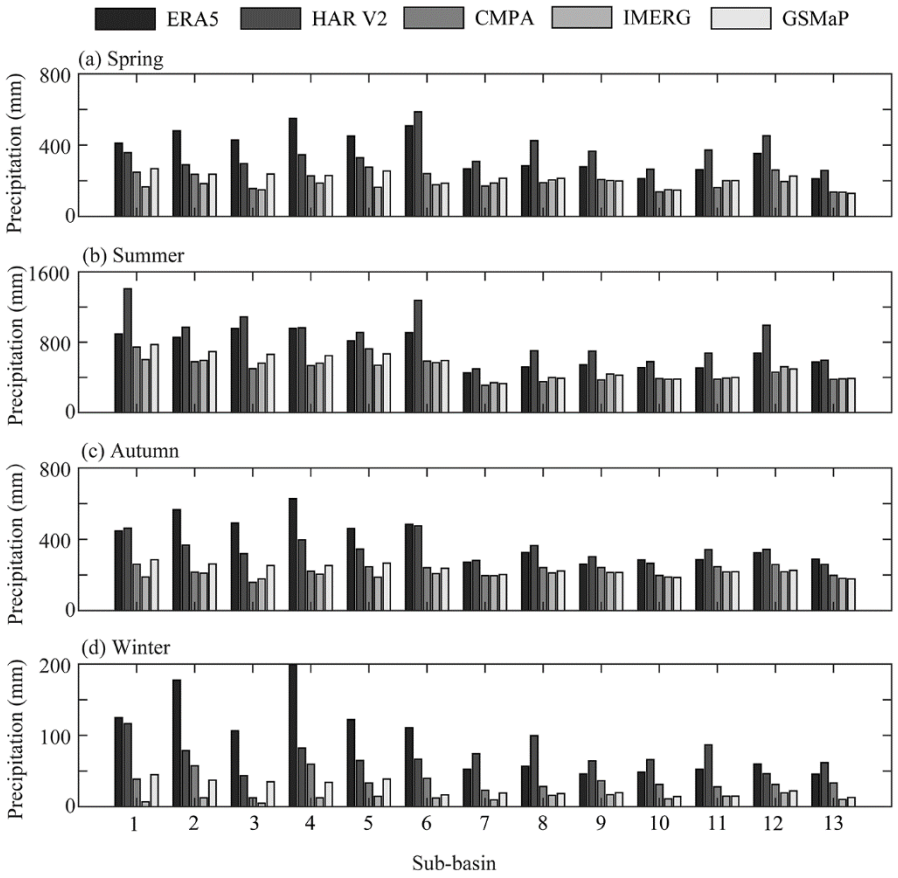

Figure 4 Comparison of the seasonal precipitation from the five products in different sub-basins of the Minjiang River basin. Spring: March to May; Summer: June to August; Autumn: September to November; Winter: December to February. The seasonal precipitation is the average value from 2008 to 2017. Note that the vertical axis ranges are not the same in each panel. The mean elevation of each sub-basin on the horizontal axis increases from left to right.

4.3 Variations of water budget components between different sub-basins

The annual average values of runoff, ET and precipitation for the 13 sub-basins are presented in Figure 5. The periods for averaging the water budget components are corresponding to the temporal coverage of runoff data in each sub-basin, as shown in Table 2.

Figure 5 shows that the runoff varies greatly between different sub-basins, ranging from a minimum of less than 400 mm/y to more than 1500 mm/y. Generally, sub-basins located in the lowland areas have higher runoff than those in the highland areas. Particularly, Figure 5 shows that the runoff of the Liusha River basin (Sub-basin 3) is much less than that of its adjacent Yingjing River basin (Sub-basin 1). The former has a runoff of 491.6 mm/y, while the latter is 1402.3 mm/y. This is

likely because the Liusha River basin is located at the leeward slope of a mountain while the Yingjing River basin is located at the windward slope, indicating the local topography has great influences on the distribution of precipitation. In terms of the ET, the ensemble mean estimates of the six ET products range from 546 mm/y in the Shouxi River basin (Sub-basin 4) to 664 mm/y in the Yingjing River basin (Sub-basin 1), showing small variability among different sub-basins.

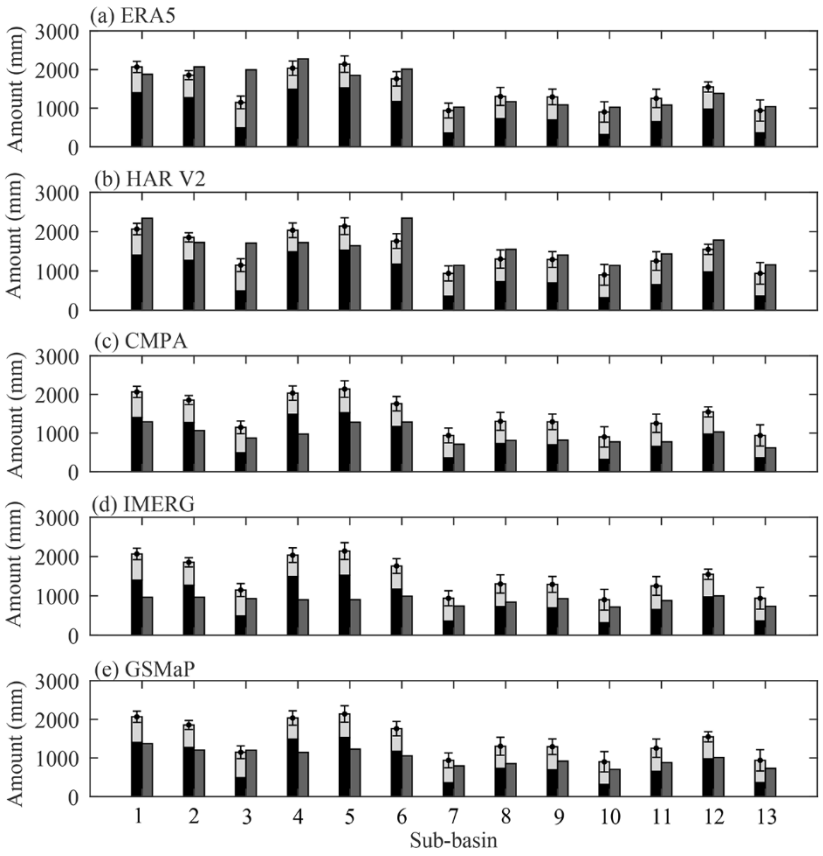

Figure 5 Comparison between the multi-year average precipitation amount from (a) ERA5, (b) HAR V2 (c) CMPA, (d) IMERG and (e) GSMaP and the sum of multi-year average runoff and ET. The periods for averaging water budget components are consistent with the temporal coverage of runoff data in each sub-basin. The black bars denote the observed runoff. The light grey bars denote the mean value of ET from the six ET products. The dark grey bars denote the precipitation from the products. The error bars denote the uncertainty in ET (the range between maximum and minimum ET estimates of the six products).

Figure 5 shows that variations of precipitation among different sub-basins for the five gridded precipitation products are generally similar to that of runoff, with high precipitation in the lowland

sub-basins but low in the highland sub-basins. However, large differences exist among these products. The precipitation amount of the two ABDs is much larger than that of SBPs. ERA5 (Figure 5a), HAR V2 (Figure 5b) and CMPA (Figure 5c) show a sharp decrease in precipitation in the Zhenjiangguan River basin (Sub-basin 7) compared with the Songlin River basin (Sub-basin 6) that is similar to the pattern of runoff, while the variability of precipitation shown in IMERG (Figure 5d) and GSMaP (Figure 5e) is much small. Particularly, almost none of the products reveal the dry condition in the Liusha River basin (Sub-basin 3), indicating these products are difficult to reflect the local-scale spatial variability of precipitation.

4.4 Water budget closure

Figure 5 also compares the sum of runoff and ET with the precipitation from the five products for the 13 sub-basins. The sum of annual runoff and ET ranges from 900.8 mm/y in the Zumuzu River basin (Sub-basin 10) to 2139.3 mm/y in the Tianquan River basin (Sub-basin 5). It can be seen that the precipitation amount from the three SBPs is clearly smaller than the sum of annual runoff and ET in almost all sub-basins (Figure 5c-e). Compared with the three SBPs, the precipitation amount from ERA5 and HAR V2 is much closer to the sum of annual runoff and ET in most sub-basins (Figure 5a-b). The differences between the precipitation amount and the sum of runoff and ET averaged across all the sub-basins (weighted by sub-basin area) are 58.0 mm/y and 204.3 mm/y for ERA5 and HAR V2, respectively.

The annual average water imbalance for the 13 sub-basins is calculated with Eq. (2) and shown in Table 3. Table 3 shows that the three SBPs yield large negative water imbalance in most sub-basins. The values of water imbalance averaged across all sub-basins (weighted by sub-basin area) are -61.2% for CMPA, -58.4% for IMERG and -56.0% for GSMaP. Similar to our results, that satellite or gauge-based precipitation products cannot close the basin-wide water budget is especially common in regions with complex-terrain, as reported in the Himalaya region (Savéan *et al*., 2015), the upper Indus (Immerzeel *et al*.,2015; Li *et al*., 2020), the Amazon basin (Moreira *et al*., 2019) and the mountainous basins in Canada (Wang et al, 2014a, 2014b, 2015) and the western United States (Henn *et al*., 2018). This may indicate the widespread deficiency in the application of satellite or gauge-based precipitation in mountainous regions. In comparison, ERA5 and HAR V2 can better close the

basin-wide water budget in the Minjiang River basin. The values of water imbalance calculated based on ERA5 are within ±30.0% in 85% of the sub-basins, with an average value across all sub-basins of 21.9%. In the Liusha River basin, ERA5 yields a large water imbalance greater than 170.0%, which may be because ERA5 has a coarse resolution and cannot give accurate precipitation estimates at a small scale. Compared with ERA5, the water budget calculated based on HAR V2 in the Liusha River basin is improved, mainly due to its relatively high resolution. HAR V2 yields positive water imbalance in most sub-basins and the average value across all sub-basins is 54.2%; nevertheless, it closes the water budget within ±30.0% of runoff in about 50% of the sub-basins, generally showing better performance than the SBPs.

Table 3 Annual average water imbalance (%, relative to runoff) calculated from five precipitation products. The water imbalance values were calculated based on multi-year average values of precipitation, ET and runoff and the averaging period in each sub-basin is corresponding to the temporal coverage of runoff data.

Sub-basin	Basin name	ERA5	HAR V2	CMPA	IMERG	GSMaP
1	Yingjing	-13.5	19.6	-55.2	-78.6	-49.4
2	Wenjing	16.9	-10.3	-62.1	-69.9	-51.1
3	Liusha	172.1	114.1	-56.1	-44.6	10.7
4	Shouxi	16.2	-21.1	-71.2	-76.2	-59.9
5	Tianquan	-19.0	-32.5	-56.2	-81.0	-59.7
6	Songlin	21.5	49.9	-40.4	-65.6	-60.0
7	Zhenjiangguan	24.6	56.9	-63.2	-54.6	-39.9
8	Heishui	-18.7	33.7	-67.7	-63.4	-61.6
9	Xiaojin	-29.5	16.1	-68.0	-52.3	-53.6
10	Zumuzu	38.6	75.3	-40.1	-58.0	-62.1
11	Suomo	-26.3	27.7	-73.4	-57.1	-56.9
12	Zheduo	-17.1	24.3	-53.2	-56.3	-55.0
13	Chuosijia	28.0	60.0	-88.1	-56.2	-57.6
Area-weighted average		21.9	54.2	-61.2	-58.4	-56.0

When calculating the water imbalance, due to the lack of ET observations, the ensemble of six ET products was used in this study, which may cause uncertainties to the analysis. The ET products include satellite-based estimates (GLEAM, MODIS and GLASS) and land surface/atmospheric model-based estimates (ERA5, HAR V2 and GLDAS). Figure 6 compares the annual average ET values from the six products in the 13 sub-basins. Among the six products, GLDAS has the largest ET with an average value of 685.9 mm/y across all sub-basins, followed by HAR V2 (666.1 mm/y), MODIS (619.8 mm/y), GLEAM (558.0 mm/y) and ERA5 (534.8 mm/y). The GLASS has the smallest ET value of 453.5 mm/y. The differences among these products are relatively small in the lowland sub-basins but large in the highland sub-basins. Overall, the differences among these products are much small compared with the uncertainties in precipitation. For most of the lowland sub-basins, the uncertainties in ET (i.e. the range between maximum and minimum ET estimates of the six products.) account for less than 20.0% of corresponding annual runoff, which are small compared with the values of water imbalance. In some highland sub-basins (Sub-basin 10 and 13) where the runoff is relatively small but ET differences among these products are large, the water budget analysis may contain some uncertainties. Nevertheless, taking all the sub-basins as a whole, the SBPs indeed severely underestimate precipitation in this region and the two ABDs are more skillful in closing the basin-wide water budget. This can also be implied from the runoff coefficients. The runoff coefficients derived from ERA5 and HAR V2 are between 0.3 and 0.7 at most sub-basins, which is accepted for humid mountainous regions (Zhan and Ye, 2000). However, the runoff coefficients calculated based on the three SBPs are larger than 0.8 at most sub-basins and even irrationally larger than 1.0 at some sub-basins.

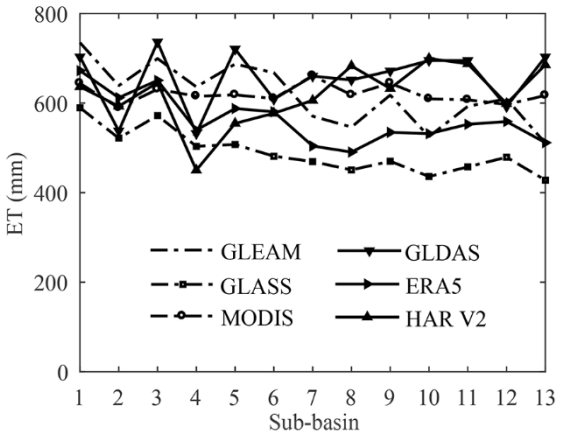

Figure 6 Basin-average evapotranspiration (ET) from six products in the 13 sub-basins of the Minjiang River basin. The values of ET are multi-year averages during the periods when runoff data are available in each sub-basin.

5. Discussions

The water budget analysis shows that the atmospheric simulation-based precipitation products (ABDs) have higher precipitation amount than satellite-based precipitation products (SBPs) and ERA5 can best close the basin-wide water budget in the Minjiang River basin. This section discusses the possible underlying reasons for the differences between the ABDs and SBPs.

5.1 Topographical dependence of the differences between SBPs and ABDs

The elevation dependence of precipitation from the five products was investigated at both gauge locations (Figure 7a) and all grid cells within the Minjiang River basin (Figure 7b). Figure 7a shows that precipitation from gauge observations increases with increasing elevations below 1500 m.s.l. and then decreases above this elevation level. Among the three SBPs, precipitation from CMPA and GSMaP show similar elevation dependence to that of gauge observations, while IMERG cannot capture the precipitation maximum around 1500 m a.s.l. In addition, it can be seen that precipitation from CMPA is much close to gauge observations at low elevations, but is significantly lower than that of gauge data above 3000 m a.s.l. This is because that CMPA has fused a large amount of rain gauge data at low elevations but less at high elevations, suggesting that the performance of satellite-gauge merged products is greatly affected by the density of rain gauges fused in them. The two ABDs generally show consistent elevation dependence with that of gauge data. At elevations lower than 500 m a.s.l., ERA5 and HAR V2 show a similar magnitude of precipitation to that of gauge data; however,

they have much higher precipitation than gauge observations at mid to high elevations, which may be partly caused by the spatial scale mismatch between rain gauge and product grid cell. As shown in Figure 1, most of the rain gauges are located in the valleys where the weather conditions are usually drier than that in hillsides and ridges of mountains (Chen *et al*., 2012; Wastl and Zängl, 2010), while the gridded precipitation represents the grid-averaged precipitation which contains the information from hillsides and ridges of mountains. In addition, wind-induced undercatch of rain gauges may also contribute to the differences. The observations used in this study were recorded with rain gauges not equipped with a wind shield. This type of rain gauge tends to miss a proportion of precipitation (Yang *et al*., 1999), especially for snowfall that is frequent in high elevations.

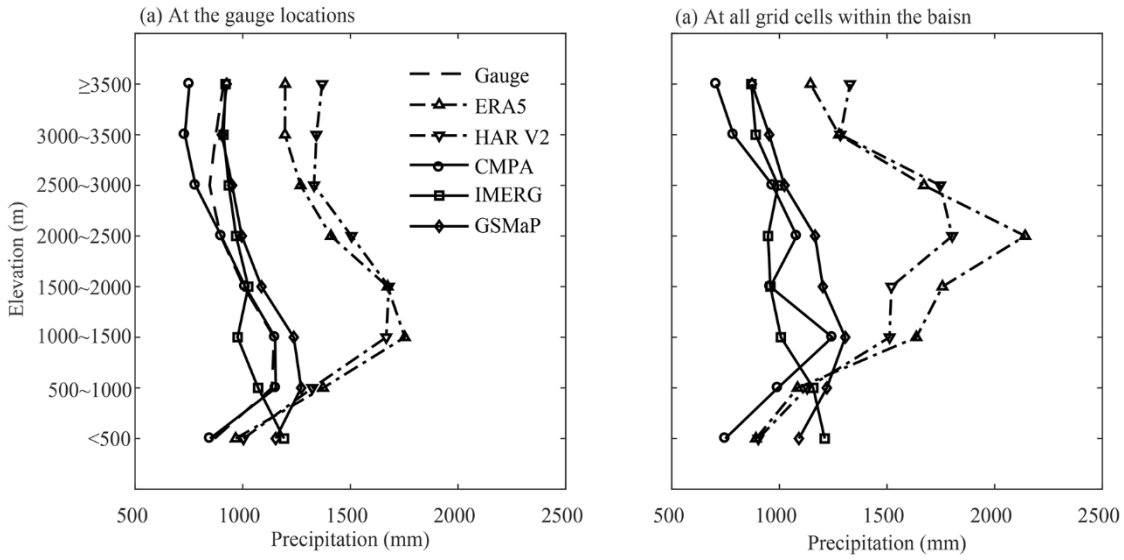

Figure 7 Elevation dependence of annual precipitation in 2017 from the five precipitation products calculated at (a) the gauge locations and (b) all grid cells within the Minjiang River basin. Figure 7a also presents the elevation dependence of precipitation from rain gauge data. All the products were firstly resampled to the spatial resolution of 0.25° × 0.25° and then the elevation dependences were compared.

Figure 7b shows the elevation dependence of precipitation for the five products calculated using all grid cells within the Mingjiang River basin. It can be seen that, for the three SBPs, the elevation dependence of precipitation calculated using all grid cells within the basin shows similar patterns to that calculated at gauge locations. In contrast, precipitation maxima in ERA5 and HAR V2 occur at a higher elevation than that shown in Figure 7a. The differences between SBPs and ABDs are quite

large at elevations between 1500 m a.s.l. and 3000 m a.s.l. This elevation range corresponds to the most complex terrain in the Minjiang River basin.

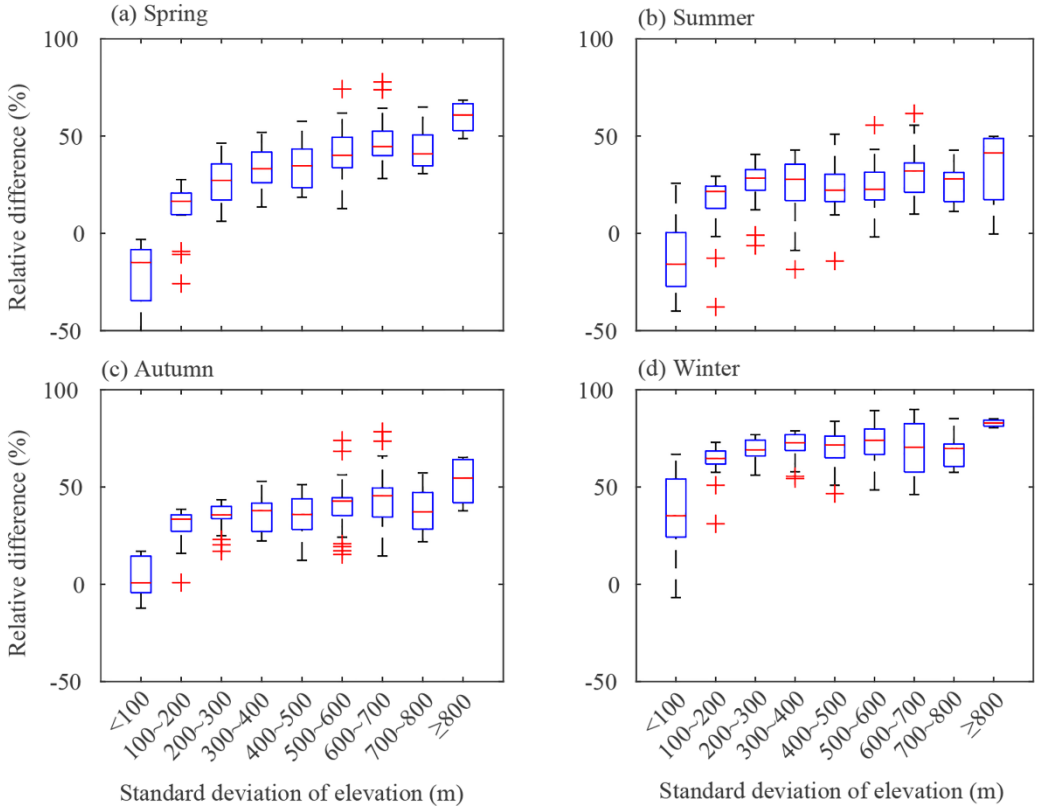

Figure 8 Relations between the precipitation differences from ERA5 and GSMaP (ERA5 minus GSMaP, relative to ERA5) and the standard deviation of elevation in (a) spring, (b) summer, (c) autumn and (d) winter. The differences were calculated at each ERA5 grid cell based on multi-year average seasonal precipitation from 2008 to 2017. The standard deviation of elevation was calculated for each ERA5 grid cell based on 90-m SRTM elevation data. Each box represents the distribution of precipitation differences from all grid cells within the given range of standard deviation of elevation. The red lines in the middle of boxes show the median values. The bottom and top edges of the box represent 25th and 75th percentiles respectively. The whiskers represent the extreme values and differences beyond the whiskers are displayed using "+".

To better clarify the topographical dependence of the differences between SBPs and ABDs, the relations between precipitation differences between ERA5 and GSMaP (relative to precipitation of ERA5) and topographic complexity were investigated and shown in Figure 8 (the differences between ERA5 and the other two SBPs show similar characteristics and thus are not presented here.). The

topographic complexity within each ERA5 grid cell is represented with the standard deviation of elevation, which is calculated based on the 90-m SRTM elevation data. The box in Figure 8 gave the distribution of precipitation differences between ERA5 and GSMaP for all grid cells falling in a given band of standard deviation of elevation. For calculating the difference between ERA5 and GSMaP, the GSMaP was firstly resampled to the spatial resolution of ERA5 using the area-weighted method. It can be seen from Figure 8 that there are significant positive relations between the differences and the standard deviations of elevation in all seasons. Significant differences mainly occur at grid cells with more complex terrain, while those with homogeneous terrain are relatively small. Given that ERA5 can better close the basin-wide water budget, Figure 8 suggests that the differences between ERA5 and GSMaP are mainly because SBPs like GSMaP cannot give reliable precipitation estimates in complex-terrain regions, which has also been reported in many previous studies (Derin *et al*., 2019; Derin and Yilmaz, 2014; Gebregiorgis and Hossain, 2013; Kenawy *et al*., 2015).

5.2 Seasonal variation of the differences between SBPs and ABDs

Figure 9a shows the relative differences between the annual average seasonal precipitation from ERA5 and GSMaP during 2008-2017. It can be seen that the precipitation from ERA5 is generally larger than that from GSMaP in all seasons but the relative differences vary greatly between different seasons. The relative difference for seasonal average precipitation is small in summer with a median value of 23.5% (or difference of 139.5 mm), while greater than 70.0% (or 37.3 mm) in winter. Although the absolute value in winter contributes small to the annual precipitation difference, the large relative difference between ERA5 and GSMaP in winter highlights the high uncertainties in precipitation products in winter. The large relative difference in winter is likely associated with solid and trace precipitation. SBPs tend to underestimate solid and trace precipitation, even for the latest IMERG product (Lu and Yong, 2018), while the atmospheric simulation is skillful in modeling solid precipitation (Lundquist *et al*., 2019; Wang *et al*., 2018). In the Minjiang River basin, it can be seen from Figure 9b that precipitation falling as snow (derived from ERA5 data) accounts for a considerable part of the annual total precipitation, particularly in the high-elevation regions where the percentage of solid precipitation is overall greater than 20.0%. In addition, the annual averaged albedo in winter in the Minjiang River basin from MODIS is shown in Figure 9c. The spatial pattern of

albedo is similar to that of the percentage of solid precipitation in ERA5, indicating that ERA5 can reasonably simulate the spatial distribution of solid precipitation. Maussion *et al*. (2014) has demonstrated that the differences between HAR and TRMM increase with an increasing proportion of snowfall, which is similar to our results because snowfall mainly occurs in winter in the Minjiang River basin.

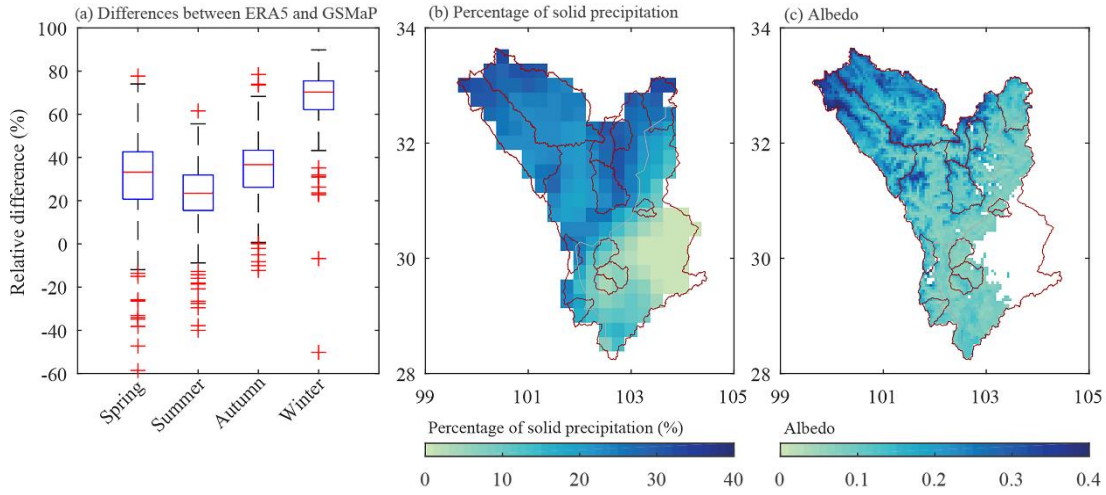

Figure 9 (a) Differences between precipitation from ERA5 and GSMaP (ERA5 minus GSMaP, relative to ERA5) in four seasons. The relative differences were calculated at each ERA5 grid cell within the Minjiang River basin based on the multi-year average seasonal precipitation from 2008 to 2017. Each box represents the distribution of relative precipitation differences from all grid cells within the Minjiang River basin. (b) Spatial pattern of the percentage of precipitation falling as solid precipitation in ERA5 in the Minjiang River basin averaged from 2008 to 2017. (c) Spatial pattern of the albedo from MODIS averaged across the winters from 2008 to 2017

6. Concluding remarks

This study investigates the performance of three satellite-based precipitation products (CMPA, IMERG and GSMaP) and two atmospheric simulation-based datasets (ERA5 and HAR V2) in the monsoon-dominated mountainous Minjiang River basin, focusing on the potential of these products in closing basin-wide water budget.

Rain gauge data show that precipitation in the Minjiang River basin is of great spatial variability. Among the three satellite-based precipitation products, precipitation from CMPA that has fused a large amount of ground data shows the best consistency with gauge observations, while both GSMaP

and IMERG yield more precipitation than gauge observations in the low elevations (<500 m a.s.l). IMERG cannot even reproduce the location of precipitation maximum. The two atmospheric simulation-based precipitation products can generally reproduce the spatial patterns of observed precipitation. The precipitation amount from ERA5 and HAR V2 is close to that from gauge observations in the low elevations but is much larger than that from gauge observations and satellite-based precipitation products in the mid to high elevations.

Assessment of water budget shows that severe negative water imbalance exists in most sub-basins when the satellite-based precipitation products are applied. The values of water imbalance averaged across all sub-basins for CMPA, IMERG and GSMaP are -61.2%, -58.4% and -56.0% of corresponding runoff, respectively, indicating that these satellite-based products cannot be directly used for hydrological applications in this region. The two atmospheric simulation-based datasets show better performance than the satellite-based products, with water imbalance values between ±30.0% in 85% (for ERA5) and 46% (for HAR V2) of the sub-basins, respectively. Further analyses show that large relative differences between satellite-based precipitation products and atmospheric simulation-based datasets mainly occur in areas with large topographic relief and in winter, which suggests that atmospheric simulation-based datasets are more skillful in estimating orographic precipitation and solid precipitation than satellite-based products in complex-terrain regions.

Although atmospheric simulation-based precipitation datasets show great potential in mountainous regions, they have some uncertainties and need further improvements. Currently, most atmospheric simulation-based precipitation products have a horizontal resolution coarser than 10 km, which cannot capture the local-scale spatial variability of precipitation and are hard to be applied in small-scale river basins, as is the case in the Liusha River basin where both ERA5 and HAR V2 overestimate precipitation a lot. Moreover, the performance of atmospheric simulation-based precipitation products is highly affected by the model's configuration and parameterization and improvements are still needed to better represent the physical processes. Recently, many studies have demonstrated that convection-permitting modeling is useful to describe the precipitation-topography relationships in mountainous regions and shows better performance than coarse-resolution modeling (Gao *et al*., 2020; Norris *et al*., 2017; Sarmadi *et al*, 2019; Wang *et al*., 2020; Zhou *et al*., 2021),

which is expected to play an important role in mountainous hydrology in the future. In addition, merging the atmospheric simulation-based precipitation datasets with other data sources may also contribute to improving their accuracy in mountainous areas.

References

Bai, P. and Liu, X. (2018) Evaluation of five satellite-based precipitation products in two gauge-scarce basins on the Tibetan Plateau. *Remote Sensing*, 10(8). https://doi.org/10.3390/RS10081316.

Becker, A., Finger, P., Meyer-Christoffer, A., Rudolf, B., Schamm, K., Schneider, U. and Ziese, M. (2013) A description of the global land-surface precipitation data products of the Global Precipitation Climatology Centre with sample applications including centennial (trend) analysis from 1901-present. *Earth System Science Data*, 5(1): 71–99. https://doi.org/10.5194/essd-5-71-2013.

Beighley, R.E., K.G.Eggert, Dunne, T., He, Y., K.L.Verdin and Gummadi1, V. (2009) Simulating hydrologic and hydraulic processes throughout the Amazon River Basin. *Hydrological Processes*, 23(November 2008): 1221–1235. https://doi.org/10.1002/hyp.

Belabid, N., Zhao, F., Brocca, L., Huang, Y. and Tan, Y. (2019) Near-real-time flood forecasting based on satellite precipitation products. *Remote Sensing*, 11(3). https://doi.org/10.3390/rs11030252.

Chen, H., Yuan, W., Li, J. and Yu, R. (2012) A possible cause for different diurnal variations of warm season rainfall as shown in station observations and TRMM 3B42 data over the southeastern Tibetan plateau. *Advances in Atmospheric Sciences*, 29(1): 193–200. https://doi.org/10.1007/s00376-011-0218-1.

Chen, Y., Sharma, S., Zhou, X., Yang, K., Li, X., Niu, X., Hu, X. and Khadka, N. (2020) Spatial performance of multiple reanalysis precipitation datasets on the southern slope of central Himalaya. *Atmospheric Research*, 105365. https://doi.org/10.1016/j.atmosres.2020.105365.

Chiang, Y.M., Hsu, K.L., Chang, F.J., Hong, Y. and Sorooshian, S. (2007) Merging multiple precipitation sources for flash flood forecasting. *Journal of Hydrology*, 340(3–4): 183–196. https://doi.org/10.1016/j.jhydrol.2007.04.007.

Cui, X., Liu, S. and Wei, X. (2012) Impacts of forest changes on hydrology: A case study of large watersheds in the upper reaches of Minjiang River watershed in China. *Hydrology and Earth System Sciences*, 16(11): 4279–4290. https://doi.org/10.5194/hess-16-4279-2012.

Derin, Y., Anagnostou, E., Berne, A., Borga, M., Boudevillain, B., Buytaert, W., Chang, C.H., Chen, H., Delrieu, G., Hsu, Y.C., Lavado-Casimiro, W., Manz, B., Moges, S., Nikolopoulos, E.I., Sahlu, D., Salerno, F., Rodríguez-Sánchez, J.P., Vergara, H.J. and Yilmaz, K.K. (2019) Evaluation of GPM-era Global Satellite Precipitation Products over Multiple Complex Terrain Regions. *Remote Sensing*, 11(24). https://doi.org/10.3390/rs11242936.

Derin, Y. and Yilmaz, K.K. (2014) Evaluation of multiple satellite-based precipitation products over complex topography. *Journal of Hydrometeorology*, 15(4): 1498–1516. https://doi.org/10.1175/JHM-D-13-0191.1.

El Kenawy, A.M., Lopez-Moreno, J.I., McCabe, M.F. and Vicente-Serrano, S.M. (2015) Evaluation of the TMPA-3B42 precipitation product using a high-density rain gauge network over complex terrain in northeastern Iberia. *Global and Planetary Change*, 133: 188–200. https://doi.org/10.1016/j.gloplacha.2015.08.013.

Farr, T.G., Crippen, B., Duren, R., Hensley, S., Kobrick, M., Paller, M., Rodriguez, E., Roth, L., Seal, D., Shaffer, S., Shimada, J., Umland, J., Werner, M., Oskin, M., Burbank, D. and Alsdor, D. (2007). The shuttle radar topography mission. *Reviews of Geophysics*, 45: RG2004. https://doi.org/10.1029/2005RG000183.

Gao, Y., Chen, F. and Jiang, Y. (2020) Evaluation of a convection-permitting modeling of precipitation over the Tibetan Plateau and its influences on the simulation of snow-cover fraction. *Journal of Hydrometeorology*, 21(7): 1531–1548. https://doi.org/10.1175/JHM-D-19-0277.1.

Gebregiorgis, A.S. and Hossain, F. (2013) Understanding the dependence of satellite rainfall uncertainty on topography and climate for hydrologic model simulation. *IEEE Transactions on Geoscience and Remote Sensing*, 51(1): 704–718. https://doi.org/10.1109/TGRS.2012.2196282.

He, X., Kim, H., Kirstetter, P.E., Yoshimura, K., Chang, E.C., Ferguson, C.R., Erlingis, J.M., Hong, Y. and Oki, T. (2015) The diurnal cycle of precipitation in regional spectral model simulations over West Africa: Sensitivities to resolution and cumulus schemes. *Weather and Forecasting*, 30(2): 424–445. https://doi.org/10.1175/WAF-D-14-00013.1.

Henn, B., Newman, A.J., Livneh, B., Daly, C. and Lundquist, J.D. (2018) An assessment of

differences in gridded precipitation datasets in complex terrain. *Journal of Hydrology*, 556: 1205–1219. https://doi.org/10.1016/j.jhydrol.2017.03.008.

Hersbach, H., Bell, B., Berrisford, P., Hirahara, S., Horányi, A., Muñoz-Sabater, J., Nicolas, J., Peubey, C., Radu, R., Schepers, D., Simmons, A., Soci, C., Abdalla, S., Abellan, X., Balsamo, G., Bechtold, P., Biavati, G., Bidlot, J., Bonavita, M., De Chiara, G., Dahlgren, P., Dee, D., Diamantakis, M., Dragani, R., Flemming, J., Forbes, R., Fuentes, M., Geer, A., Haimberger, L., Healy, S., Hogan, R.J., Hólm, E., Janisková, M., Keeley, S., Laloyaux, P., Lopez, P., Lupu, C., Radnoti, G., de Rosnay, P., Rozum, I., Vamborg, F., Villaume, S. and Thépaut, J.N. (2020) The ERA5 global reanalysis. *Quarterly Journal of the Royal Meteorological Society*, 146(730): 1999–2049. https://doi.org/10.1002/qj.3803.

Hong, Y., Adler, R.F., Negri, A. and Huffman, G.J. (2007) Flood and landslide applications of near real-time satellite rainfall products. *Natural Hazards*, 43(2): 285–294. https://doi.org/10.1007/s11069-006-9106-x.

Hou, A.Y., Kakar, R.K., Neeck, S., Azarbarzin, A.A., Kummerow, C.D., Kojima, M., Oki, R., Nakamura, K. and Iguchi, T. (2014) The global precipitation measurement mission. *Bulletin of the American Meteorological Society*, 95(5): 701–722. https://doi.org/10.1175/BAMS-D-13-00164.1.

Hu, X. and Yuan, W. (2021) Evaluation of ERA5 precipitation over the eastern periphery of the Tibetan plateau from the perspective of regional rainfall events. *International Journal of Climatology*, 41(4): 2625–2637. https://doi.org/10.1002/joc.6980.

Huffman, G.J., Adler, R.F., Bolvin, D.T., Gu, G., Nelkin, E.J., Bowman, K.P., Hong, Y., Stocker, E.F. and Wolff, D.B. (2007) The TRMM Multisatellite Precipitation Analysis (TMPA): Quasi-global, multiyear, combined-sensor precipitation estimates at fine scales. *Journal of Hydrometeorology*, 8(1): 38–55. https://doi.org/10.1175/JHM560.1.

Huffman, G.J., Bolvin, D.T., Nelkin, E.J. and Tan, J. (2019) *Integrated Multi-satellitE Retrievals for GPM (IMERG) Technical Documentation*. *NASA*.

Hughes, D.A. (2006) An evaluation of the potential use of satellite rainfall data for input to water resource estimation models in southern Africa. *IAHS-AISH Publication*, (308): 75–80.

Immerzeel, W.W., Wanders, N., Lutz, A.F., Shea, J.M. and Bierkens, M.F.P. (2015) Reconciling high-altitude precipitation in the upper Indus basin with glacier mass balances and runoff. *Hydrology and Earth System Sciences*, 19(11): 4673–4687. https://doi.org/10.5194/hess-19-4673-2015.

Joyce, R.J., Janowiak, J.E., Arkin, P.A. and Xie, P. (2004) CMORPH: A method that produces global precipitation estimates from passive microwave and infrared data at high spatial and temporal resolution. *Journal of Hydrometeorology*, 5(3): 487–503. https://doi.org/10.1175/1525-7541(2004)005<0487:CAMTPG>2.0.CO;2.

Keller, J.D. and Wahl, S. (2020) Representation of Climate in Reanalyses - An Intercomparison for Europe and North America. *Journal of Climate*, 1–62. https://doi.org/10.1175/jcli-d-20-0609.1.

Kubota, T., Hashizume, H., Shige, S., Okamoto, K., Aonashi, K., Takahashi, N., Ushio, T. and Kachi, M. (2006) Global precipitation map using satelliteborne microwave radiometers by the GSMaP project: Production and validation. *International Geoscience and Remote Sensing Symposium (IGARSS)*, 45(7): 2584–2587. https://doi.org/10.1109/IGARSS.2006.668.

Li, D., Yang, K., Tang, W., Li, X., Zhou, X. and Guo, D. (2020) Characterizing precipitation in high altitudes of the western Tibetan plateau with a focus on major glacier areas. *International Journal of Climatology*, (August 2019): 1–14. https://doi.org/10.1002/joc.6509.

Li, X. (2014) Characterization, controlling, and reduction of uncertainties in the modeling and observation of land-surface systems. *Science China Earth Sciences*, 57(1): 80–87. https://doi.org/10.1007/s11430-013-4728-9.

Li, Z., Yang, D., Gao, B., Jiao, Y., Hong, Y. and Xu, T. (2015) Multiscale hydrologic applications of the latest satellite precipitation products in the Yangtze river basin using a distributed hydrologic model. *Journal of Hydrometeorology*, 16(1): 407–426. https://doi.org/10.1175/JHM-D-14-0105.1.

Liu, T., Yang, K., Qin, J., and Tian, F. (2018) Construction and Applications of Time Series of Monthly Precipitation at Weather Stations in the Central and Eastern Qinghai-Tibetan Plateau. *Plateau Meteorology*, 37, 1449–1457. https://doi.org/10．7522／j．issn．1000－0534．2018．00060

Liu, X., Yang, T., Hsu, K., Liu, C. and Sorooshian, S. (2017) Evaluating the streamflow simulation capability of PERSIANN-CDR daily rainfall products in two river basins on the Tibetan Plateau. *Hydrology and Earth System Sciences*, 21(1): 169–181. https://doi.org/10.5194/hess-21-169-2017.

Lu, D. and Yong, B. (2018) Evaluation and hydrological utility of the latest GPM IMERG V5 and GSMaP V7 precipitation products over the Tibetan Plateau. *Remote Sensing*, 10(12). https://doi.org/10.3390/rs10122022.

Lundquist, J., HugHes, M., Gutmann, E. and KapnicK, S. (2019) Our skill in modeling mountain rain and snow is bypassing the skill of our observational networks. *Bulletin of the American Meteorological Society*, (December): 2473–2490. https://doi.org/10.1175/BAMS-D-19-0001.1.

Maussion, F., Scherer, D., Mölg, T., Collier, E., Curio, J. and Finkelnburg, R. (2014) Precipitation seasonality and variability over the Tibetan Plateau as resolved by the high Asia reanalysis. *Journal of Climate*, 27(5): 1910–1927. https://doi.org/10.1175/JCLI-D-13-00282.1.

Miralles, D.G., Holmes, T.R.H., De Jeu, R.A.M., Gash, J.H., Meesters, A.G.C.A. and Dolman, A.J. (2011) Global land-surface evaporation estimated from satellite-based observations. *Hydrology and Earth System Sciences*, 15(2): 453–469. https://doi.org/10.5194/hess-15-453-2011.

Monteith, J.L. (1965) Evaporation and environment. *Symposia of the Society for Experimental Biology*.

Moreira, A.A., Ruhoff, A.L., Roberti, D.R., Souza, V. de A., da Rocha, H.R. and Paiva, R.C.D. de. (2019) Assessment of terrestrial water balance using remote sensing data in South America. *Journal of Hydrology*, 575(December 2018): 131–147. https://doi.org/10.1016/j.jhydrol.2019.05.021.

Norris, J., Carvalho, L.M.V., Jones, C., Cannon, F., Bookhagen, B., Palazzi, E. and Tahir, A.A. (2017) The spatiotemporal variability of precipitation over the Himalaya: evaluation of one-year WRF model simulation. *Climate Dynamics*, 49(5–6): 2179–2204. https://doi.org/10.1007/s00382-016-3414-y.

Pritchard, D.M.W., Forsythe, N., Fowler, H.J., O'Donnell, G.M. and Li, X.F. (2019) Evaluation of upper indus near-surface climate representation by WRF in the High Asia Refined Analysis.

Journal of Hydrometeorology, 20(3): 467–487. https://doi.org/10.1175/JHM-D-18-0030.1.

Rienecker, M.M., Suarez, M.J., Gelaro, R., Todling, R., Bacmeister, J., Liu, E., Bosilovich, M.G., Schubert, S.D., Takacs, L., Kim, G.K., Bloom, S., Chen, J., Collins, D., Conaty, A., Da Silva, A., Gu, W., Joiner, J., Koster, R.D., Lucchesi, R., Molod, A., Owens, T., Pawson, S., Pegion, P., Redder, C.R., Reichle, R., Robertson, F.R., Ruddick, A.G., Sienkiewicz, M. and Woollen, J. (2011) MERRA: NASA's modern-era retrospective analysis for research and applications. *Journal of Climate*, 24(14): 3624–3648. https://doi.org/10.1175/JCLI-D-11-00015.1.

Rodell, M., Houser, P.R., Jambor, U., Gottschalck, J., Mitchell, K., Meng, C.J., Arsenault, K., Cosgrove, B., Radakovich, J., Bosilovich, M., Entin, J.K., Walker, J.P., Lohmann, D. and Toll, D. (2004) The Global Land Data Assimilation System. *Bulletin of the American Meteorological Society*, 85(3): 381–394. https://doi.org/10.1175/BAMS-85-3-381.

Sarmadi, F., Huang, Y., Thompson, G., Siems, S.T. and Manton, M.J. (2019) Simulations of orographic precipitation in the Snowy Mountains of Southeastern Australia. *Atmospheric Research*, 219(December 2018): 183–199. https://doi.org/10.1016/j.atmosres.2019.01.002.

Savéan, M., Delclaux, F., Chevallier, P., Wagnon, P., Gonga-Saholiariliva, N., Sharma, R., Neppel, L. and Arnaud, Y. (2015) Water budget on the Dudh Koshi River (Nepal): Uncertainties on precipitation. *Journal of Hydrology*, 531: 850–862. https://doi.org/10.1016/j.jhydrol.2015.10.040.

Schaaf, C.B., Gao, F., Strahler, A.H., Lucht, W., Li, X., Tsang, T., Strugnell, N.C., Zhang, X., Jin, Y., Muller, J.-P., Lewis, P., Barnsley, M., Hobson, P., Disney, M., Roberts, G., Dunderdale, M., Doll, C., d'Entremont, R.P., Hu, B., Liang, S., Privette, J.L. and Roy, D. (2002). First operational BRDF, albedo nadir reflectance products from MODIS. *Remote Sensing of Environment*, 83(1): 135–148. https://doi.org/https://doi.org/10.1016/S0034-4257(02)00091-3.

Serrano-Notivoli, R., de Luis, M. and Beguería, S. (2017) An R package for daily precipitation climate series reconstruction. *Environmental Modelling and Software*, 89: 190–195. https://doi.org/10.1016/j.envsoft.2016.11.005.

Shen, Y., Xiong, A., Hong, Y., Yu, J., Pan, Y., Chen, Z. and Saharia, M. (2014a) Uncertainty analysis of five satellite-based precipitation products and evaluation of three optimally merged multi-

algorithm products over the Tibetan Plateau. *International Journal of Remote Sensing*, 35(19): 6843–6858. https://doi.org/10.1080/01431161.2014.960612.

Shen, Y., Zhao, P., Pan, Y. and Yu, J. (2014b) A high spatiotemporal gauge-satellite merged precipitation analysis over China. *Journal of Geophysical Research*, 3063–3075. https://doi.org/10.1002/2013JD020686.

Shige, S., Kida, S., Ashiwake, H., Kubota, T. and Aonashi, K. (2013) Improvement of TMI rain retrievals in mountainous areas. *Journal of Applied Meteorology and Climatology*, 52(1): 242–254. https://doi.org/10.1175/JAMC-D-12-074.1.

Siddique-E-Akbor, A.H.M., Hossain, F., Sikder, S., Shum, C.K., Tseng, S., Yi, Y., Turk, F.J. and Limaye, A. (2014) Satellite Precipitation Data–Driven Hydrological Modeling for Water Resources Management in the Ganges, Brahmaputra, and Meghna Basins. *Earth Interactions*, 18(17): 1–25. https://doi.org/10.1175/ei-d-14-0017.1.

Su, F., Hong, Y. and Lettenmaier, D.P. (2008) Evaluation of TRMM multisatellite precipitation analysis (TMPA) and its utility in hydrologic prediction in the La Plata Basin. *Journal of Hydrometeorology*, 9(4): 622–640. https://doi.org/10.1175/2007JHM944.1.

Sun, H., Su, F., He, Z., Ou, T., Chen, D., Li, Z. and Li, Y. (2021) Hydrological evaluation of high-resolution precipitation estimates from the WRF model in the Third Pole river basins. *Journal of Hydrometeorology*. https://doi.org/10.1175/jhm-d-20-0272.1.

Tarek, M., Brissette, F.P. and Arsenault, R. (2020) Evaluation of the ERA5 reanalysis as a potential reference dataset for hydrological modelling over North America. *Hydrology and Earth System Sciences*, 24(5): 2527–2544. https://doi.org/10.5194/hess-24-2527-2020.

Wang, D., Wang, G. and Anagnostou, E.N. (2005) Use of satellite-based precipitation observation in improving the parameterization of canopy hydrological processes in land surface models. *Journal of Hydrometeorology*, 6(5): 745–763. https://doi.org/10.1175/JHM438.1.

Wang, S., Huang, J., Li, J., Rivera, A., McKenney, D.W. and Sheffield, J. (2014a) Assessment of water budget for sixteen large drainage basins in Canada. *Journal of Hydrology*, 512: 1–15. https://doi.org/10.1016/j.jhydrol.2014.02.058.

Wang, S., Huang, J., Yang, D., Pavlic, G. and Li, J. (2015) Long-term water budget imbalances and

error sources for cold region drainage basins. *Hydrological Processes*, 29(9): 2125–2136. https://doi.org/10.1002/hyp.10343.

Wang, S., McKenney, D.W., Shang, J. and Li, J. (2014b) A national-scale assessment of long-term water budget closures for Canada's watersheds. *Journal of Geophysical Research*, (3): 6578–6595. https://doi.org/10.1002/2014JD021488.

Wang, X., Tolksdorf, V., Otto, M. and Scherer, D. (2020) WRF-based dynamical downscaling of ERA5 reanalysis data for High Mountain Asia: Towards a new version of the High Asia Refined analysis. *International Journal of Climatology*, (May): 1–20. https://doi.org/10.1002/joc.6686.

Wang, Y., Geerts, B. and Liu, C. (2018) A 30-year convection-permitting regional climate simulation over the interior western United States. Part I: Validation. *International Journal of Climatology*, 38(9): 3684–3704. https://doi.org/10.1002/joc.5527.

Wang, Y., Yang, K., Zhou, X., Chen, D., Lu, H., Ouyang, L., Chen, Y., Lazhu and Wang, B. (2020) Synergy of orographic drag parameterization and high resolution greatly reduces biases of WRF-simulated precipitation in central Himalaya. *Climate Dynamics*, 54(3–4): 1729–1740. https://doi.org/10.1007/s00382-019-05080-w.

Wastl, C. and Zängl, G. (2010) Mountain-valley precipitation differences in the northern Alps: An exemplary high-resolution modeling study. *Meteorology and Atmospheric Physics*, 29–42.

Wu, H., Adler, R.F., Tian, Y., Huffman, G.J., Li, H. and Wang, J. (2014) Real-time global flood estimation using satellite-based precipitation and a coupled land surface and routing model Huan. *Journal of the American Water Resources Association*, 5(3): 2693–2717. https://doi.org/10.1111/j.1752-1688.1969.tb04897.x.

Xie, P., Yatagai, A., Chen, M., Hayasaka, T., Fukushima, Y., Liu, C. and Yang, S. (2007) A gauge-based analysis of daily precipitation over East Asia. *Journal of Hydrometeorology*, 8(3): 607–626. https://doi.org/10.1175/JHM583.1.

Yamamoto, M.K. and Shige, S. (2015) Implementation of an orographic/nonorographic rainfall classification scheme in the GSMaP algorithm for microwave radiometers. *Atmospheric Research*, 163: 36–47. https://doi.org/10.1016/j.atmosres.2014.07.024.

Yang, D., Goodison, B.E., Metcalfe, J.R., Louie, P., Leavesley, G., Emerson, D., Hanson, C.L.,

Golubev, V.S., Elomaa, E., Gunther, T., Pangburn, T., Kang, E. and Milkovic, J. (1999) Quantification of precipitation measurement discontinuity induced by wind shields on national gauges. *Water Resources Research*, 35(2): 491–508. https://doi.org/10.1029/1998WR900042.

Yang, N., Zhang, K., Hong, Y., Zhao, Q., Huang, Q., Xu, Y., Xue, X. and Chen, S. (2017) Evaluation of the TRMM multisatellite precipitation analysis and its applicability in supporting reservoir operation and water resources management in Hanjiang basin, China. *Journal of Hydrology*, 549: 313–325. https://doi.org/10.1016/j.jhydrol.2017.04.006.

Yao, Y., Liang, S., Cheng, J., Liu, S., Fisher, J.B., Zhang, X., Jia, K., Zhao, X., Qin, Q., Zhao, B., Han, S., Zhou, G., Zhou, G., Li, Y. and Zhao, S. (2013) MODIS-driven estimation of terrestrial latent heat flux in China based on a modified Priestley-Taylor algorithm. *Agricultural and Forest Meteorology*, 171–172: 187–202. https://doi.org/10.1016/j.agrformet.2012.11.016.

Yatagai, A., Kamiguchi, K., Arakawa, O., Hamada, A., Yasutomi, N. and Kitoh, A. (2012) Aphrodite: constructing a long-term daily gridded precipitation dataset for Asia based on a dense network of rain gauges. *Bulletin of the American Meteorological Society*, 93(9): 1401–1415. https://doi.org/10.1175/BAMS-D-11-00122.1.

Ye, B., Yang, D. and Ma, L. (2012) Effect of precipitation bias correction on water budget calculation in Upper Yellow River, China. *Environmental Research Letters*, 7(2). https://doi.org/10.1088/1748-9326/7/2/025201.

Yilmaz, K.K., Hogue, T.S., Hsu, K.L., Sorooshian, S., Gupta, H. V. and Wagener, T. (2005) Intercomparison of rain gauge, radar, and satellite-based precipitation estimates with emphasis on hydrologic forecasting. *Journal of Hydrometeorology*, 6(4): 497–517. https://doi.org/10.1175/JHM431.1.

Yuan, X., Yang, K., Hui, L., Jie, H., Sun, J. and Wang, Y. (2021) Characterizing the features of precipitation for the Tibetan Plateau among four gridded datasets: Detection accuracy and spatio-temporal variabilities. *Atmospheric Research*, 264(August): 105875. https://doi.org/10.1016/j.atmosres.2021.105875.

Zhan, D. and Ye, S. (2000) Engineering Hydrology, Beijing: China Water & Power Press.

Zhang, X., Zhang, W., and Jiang, H. (2018) Evaluation and Correction of Satellite Precipitation

Products in the Sourtheastern Tibetan Plateau Based on Basin Water Balance. *Geography and Geo-Information Science*, 34, 35–41. https://doi.org/doi:10.3969/j.issn.1672-0504.2018.06.006

Zhou, X., Yang, K., Ouyang, L., Wang, Y., Jiang, Y., Li, X., Chen, D. and Prein, A. (2021) Added value of kilometer-scale modeling over the third pole region: a CORDEX-CPTP pilot study. *Climate Dynamics*. https://doi.org/10.1007/s00382-021-05653-8.

Atmospheric simulation-based precipitation datasets outperform satellite-based products in closing basin-wide water budget in the eastern Tibetan Plateau

Yaozhi Jiang, Kun Yang*, Xiaodong Li, Wenjiang Zhang, Yan Shen, Yingying Chen, Xin Li

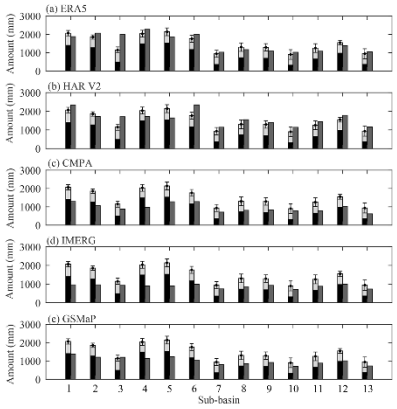

Five gridded precipitation datasets were assessed in a typical complex-terrain river basin located in the eastern Tibetan Plateau. The results support that the atmospheric simulation-based datasets can better close the basin-wide water budget than the satellite-based datasets that are generally considered to be more reliable. In the figure, the black bars denote the observed runoff; the light grey bars denote the evapotranspiration; the dark grey bars denote the precipitation from the datasets.